Solid phase diagram of a classical electronic bilayer

J.-J. Weis and D. Levesque
Laboratoire de Physique Théorique, UMR 8627, Bâtiment 210, Université de Paris-Sud, 91405 Orsay Cedex, France

S. Jorge
Departamento de Química Física I, Universidad Complutense, E-28040 Madrid, Spain
and Instituto de Química Física Rocasolano, CSIC, Serrano 119, E-28006 Madrid, Spain
(Received 2 June 2000; published 3 January 2001)

Using a Monte Carlo method in which the shape of the simulation cell can vary, we identify the sequence of crystal phases occurring in a finite-temperature strongly coupled classical electronic bilayer as the layer separation is increased. The limits of stability of the different phases are estimated and compared with ground-state calculations. Contact is made with recent experiments on two-dimensional ion plasmas.

DOI: 10.1103/PhysRevB.63.045308 PACS number(s): 73.21.−b, 64.70.Kb

I. INTRODUCTION

Strongly coupled electronic bilayers of charged particles occurring, for instance, in two-dimensional semiconductor heterostructures, dusty plasmas, or laser-beam-cooled trapped-ion plasmas benefited recently from extended experimental and theoretical studies disclosing a wide variety of structural phases.[1] Lattice dynamics calculations by Goldoni and Peeters[2] showed that the ground state of a classical bilayer Wigner crystal (one component plasma in a neutralizing uniform background) adopts five different phases depending on the separation h between the two layers. In order of increasing value of h, these phases are: a monolayer hexagonal lattice (I) ($h=0$), a staggered rectangular lattice (II), a staggered square lattice (III), a staggered rhombic lattice (IV), and a staggered hexagonal lattice (V). These authors also addressed the nonzero temperature phase diagram, and determined the stability and melting of the five structures within the harmonic approximation.[2] In later work,[3] estimates of the melting temperatures of the different phases identified in Ref. 2 were refined using canonical Monte Carlo simulations. It was shown, for instance, that the square phase corresponding to layer separations of 0.5–1 mean distance between charges melts at a temperature 35% higher than that of the hexagonal single layer system. However, in these calculations it was assumed that the ranges of stability of the different phases are those determined for the ground state.

The aim of the present work is to establish the relative stability of the crystal phases of the bilayer system at finite temperature. To this end we perform numerical simulations in an ensemble similar (but not identical) to the canonical ensemble. In each layer the cell containing the charges, the rhombus, or the rectangle, with periodic boundary conditions, has a constant area but its shape is variable. In such an ensemble the system of charges can, by modifying the aspect ratio of the edges of the cell or the angle between adjacent edges, undergo a transition to the most stable crystalline phase for a given layer separation. This method is similar to that proposed by Parrinello and Rahman[4] and Yashonath and Rao[5] to study polymorphic transitions in single crystals, but has been adapted to take account of the thermodynamic instability of the one component plasma (OCP) at low temperatures when the density of the compensating background is not kept fixed.[6]

In this paper we present Monte Carlo results for the energy and crystal phases of the bilayer Wigner crystal as a function of separation of the two layers. In contrast to the lattice dynamics calculations of Goldoni and Peeters, no *a priori* assumptions of the lattice structures are needed. By allowing the shape of the simulation cell to vary, the system can adjust to a lattice structure which gives the lowest free energy (within the constraints of finite size and periodic boundary conditions).

Our model and details of the Monte Carlo (MC) calculations are presented in Sec. II. The different crystal phases and their range of stability are identified as a function of layer separation in Sec. III. Comparison with related work is given in Sec. IV.

II. MODEL AND MONTE CARLO SIMULATIONS

In our MC simulations $N=2N_l$ point ions interacting by a $1/r$ Coulomb potential are evenly distributed in two layers L_1 and L_2 separated by a distance h. Charge neutrality is guaranteed by embedding the ions in a uniform background of opposite charge. In each layer the basic simulation cell has a variable shape, and periodic boundary conditions are imposed. The particles are not allowed to move out of the planes.

A thermodynamic state of the system is entirely specified by the dimensionless parameters $\Gamma=e^2/kTa$, and h/a where e is the ionic charge, T the temperature, k Boltzmann's constant, and a the ion-disk radius defined by $\pi\rho_l a^2=1$. The ion density in each layer is $\rho_l=N_l/\Omega$, where Ω is the area of the basic simulation cell. Choosing a as unit of length, as will be the case throughout the paper, the density in each layer takes the value $1/\pi$.

The energy of the bilayer system can be written, using an Ewald summation method, to take account of the long range of the Coulomb potential[7] and separate the intralayer and interlayer contributions, as

$$U=U_{intra}+U_{inter}, \tag{1}$$

where

$$U_{intra}=\frac{e^2}{2}\Bigg\{\sum_{i\in L_1}^{N_l}\sum_{j\in L_1}^{N_l}{\sum_{\boldsymbol{n}}}'\frac{\mathrm{erfc}(\alpha|\boldsymbol{r}_{ij}+\boldsymbol{t}\cdot\boldsymbol{n}|)}{|\boldsymbol{r}_{ij}+\boldsymbol{t}\cdot\boldsymbol{n}|}+\frac{1}{\Omega}\sum_{i\in L_1}^{N_l}\sum_{\substack{j\in L_1\\ j\neq i}}^{N_l}\sum_{\boldsymbol{G}\neq 0}\frac{2\pi}{G}\,\mathrm{erfc}(G/2\alpha)e^{i\boldsymbol{G}\cdot(\boldsymbol{\rho}_j-\boldsymbol{\rho}_i)}-\frac{1}{\Omega}\sum_{i\in L_1}^{N_l}\sum_{\substack{j\in L_1\\ j\neq i}}^{N_l}\frac{2\sqrt{\pi}}{\alpha}\Bigg\}-\frac{1}{2}C_w+\text{similar contribution with } i,j\in L_2 \tag{2}$$

and

$$U_{inter}=e^2\Bigg\{\sum_{i\in L_1}^{N_l}\sum_{j\in L_2}^{N_l}\sum_{\boldsymbol{n}}\frac{\mathrm{erfc}(\alpha|\boldsymbol{r}_{ij}+\boldsymbol{t}\cdot\boldsymbol{n}|)}{|\boldsymbol{r}_{ij}+\boldsymbol{t}\cdot\boldsymbol{n}|}+\frac{1}{\Omega}\sum_{i\in L_1}^{N_l}\sum_{j\in L_2}^{N_l}\sum_{\boldsymbol{G}\neq 0}\frac{\pi}{G}\Bigg[e^{Gh}\,\mathrm{erfc}\Big(\frac{G}{2\alpha}+\alpha h\Big)+e^{-Gh}\,\mathrm{erfc}\Big(\frac{G}{2\alpha}-\alpha h\Big)\Bigg]e^{i\boldsymbol{G}\cdot(\boldsymbol{\rho}_j-\boldsymbol{\rho}_i)}+\frac{1}{\Omega}\sum_{i\in L_1}^{N_l}\sum_{j\in L_2}^{N_l}\Bigg[2\pi h\,\mathrm{erfc}(\alpha h)-\frac{2\sqrt{\pi}}{\alpha}e^{-\alpha^2h^2}\Bigg]\Bigg\}. \tag{3}$$

In these equations, $\boldsymbol{r}_{ij}=\boldsymbol{r}_i-\boldsymbol{r}_j$, where the position of particle i is represented by a three-dimensional vector $\boldsymbol{r}_i$ having projection $\boldsymbol{\rho}_i$ on the lattice plane.

The term $-\frac{1}{2}C_w$ is the self-energy of one plane given by

$$C_w=e^2N_l\Bigg\{-\sum_{\boldsymbol{n}\neq 0}\frac{\mathrm{erfc}(\alpha|\boldsymbol{t}\cdot\boldsymbol{n}|)}{|\boldsymbol{t}\cdot\boldsymbol{n}|}-\frac{1}{\Omega}\sum_{\boldsymbol{G}\neq 0}\frac{2\pi}{G}\,\mathrm{erfc}(G/2\alpha)+\frac{2\alpha}{\sqrt{\pi}}+\frac{2\sqrt{\pi}}{\Omega\alpha}\Bigg\}. \tag{4}$$

In Eq. (2) the prime in the sum over $\boldsymbol{n}=(n_x,n_y)$ (n_x,n_y integers) means that the terms $i=j$ must be omitted when $\boldsymbol{n}=0$. Expressions (2) and (3) apply for an arbitrary oblique simulation cell characterized by two basis vectors $\boldsymbol{b}_1$ and $\boldsymbol{b}_2$ of variable lengths L_x and L_y and variable angle γ. The cell basis matrix $\boldsymbol{t}$ is given by

$$\boldsymbol{t}=\begin{pmatrix}L_x & L_y\cos\gamma\\ 0 & L_y\sin\gamma\end{pmatrix}, \tag{5}$$

and the volume of the simulation cell is $\Omega=L_xL_y\sin\gamma$. The wave vectors $\boldsymbol{G}$ which enter the reciprocal space contributions to the energy are of the form

$$\boldsymbol{G}=2\pi({}^t\boldsymbol{t})^{-1}\boldsymbol{n}, \tag{6}$$

where ${}^t\boldsymbol{t}$ denotes the transpose of $\boldsymbol{t}$, with components

$$G_x=\frac{2\pi}{\Omega}L_x\sin\gamma n_x, \tag{7}$$

$$G_y=\frac{2\pi}{\Omega}(-L_y\cos\gamma n_x+L_xn_y), \tag{8}$$

and modulus

$$G=\sqrt{G_x^2+G_y^2}. \tag{9}$$

In our calculations the sums in reciprocal space extended over all lattice vectors $\boldsymbol{G}$ subject to $|\boldsymbol{n}|^2\leqslant n_{max}^2=100$ or 400. For larger values of n_{max} the Fourier components in Eqs. (2) and (3) were negligible for all box dimensions considered.

Care has to be taken to properly choose the α parameter which governs the rate of convergence of the real- and reciprocal-space contributions in Eqs. (2) and (3). It is generally taken sufficiently large so that only the terms with $\boldsymbol{n}=0$ need to be retained in Eqs. (2) and (3), implying that the real-space term vanishes at a distance corresponding to the smallest distance from the cell center to the cell edges. The requirement, therefore, especially in the case of a rhombic simulation cell with small γ, of a large value of α and concomitantly a large number of $\boldsymbol{G}$ vectors to guarantee the independence of U on α, motivated the use, in our computations, of a rectangular simulation cell.

In the MC procedure the box characteristics L_x, L_y, and γ, taken to be identical in the two layers, were not sampled independently but by keeping the area Ω constant. This constraint was necessary to avoid the collapse of the system at high density (or equivalently low temperature) where the pressure of the OCP becomes negative,[6] and precludes the use of the isobaric ensemble to study the stability of the crystalline phases.

Different crystalline structures were identified from snapshots of instantaneous configurations; intralayer g_{11} and interlayer g_{12} pair distribution functions (PDF's) corresponding to particles in the same layer and to particles belonging to different layers but positions projected onto the same plane, respectively; coordination numbers; and order parameters. Suitable order parameters for characterizing the square and hexagonal structures are

$$\Psi_m=\Big\langle\frac{1}{N_l}\sum_{i}^{N_l}|\psi_m(i)|\Big\rangle, \tag{10}$$

where

$$\psi_m=\frac{1}{N_i}\sum_{k}^{N_i}e^{-im\theta_{ik}} \tag{11}$$

($m=4$ and 6).

The sum in Eq. (11) is taken over the N_i neighbors of particle i within the first shell of the intralayer pair distribution function; θ_{ik} is the angle between the bond of particles i and k and an arbitrary reference axis, and $\langle\cdot\rangle$ denotes an ensemble average.

In view of finite-size effects encountered for a 512-particle system for $h>1$ (see below) most simulations were performed with the larger number of ions $N=1800$ ions at the two values of the coupling parameter $\Gamma=196$ and 324 for which the single-layer electron system is well inside the solid

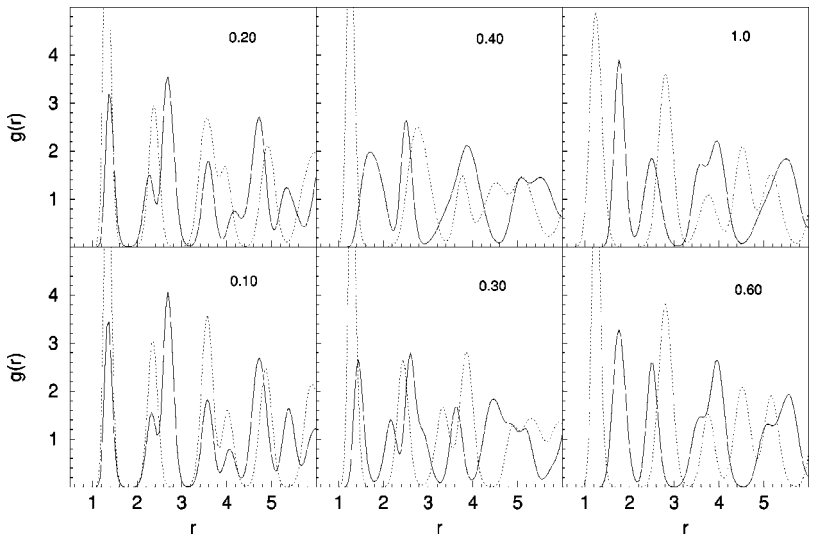

FIG. 1. Intralayer PDF $g_{11}(r)$ (solid line) and interlayer PDF $g_{12}(r)$ (dotted line) at $\Gamma=196$ for $0.1\leqslant h\leqslant 1.0$. Distances are in units of the ion-disk radius a.

phase. Melting of the quasi-two-dimensional electron solid was estimated both experimentally[8] and by computer simulation[9] to occur in the range $120<\Gamma_m<140$. A MC run involved typically of the order of 80 000 (1800 ions) or 200 000 (512 ions) cycles (after equilibration of the system), each cycle corresponding to displacement of the N ions and one change of the box dimensions keeping the volume fixed.

III. RESULTS

The simulations were started at small values of h, choosing initial conditions compatible with the fact that, for $h=0$, the monolayer of $N=2N_l$ ions must crystallize in a hexagonal lattice. This can be achieved by fixing the ions in the two layers at the sites of two rectangular lattices with an aspect ratio $\sqrt{3}$, such that the sites of one lattice sit at the centers of the cells of the other lattice. Obviously a hexagonal lattice is recovered in this way when $h\rightarrow 0$. This staggered rectangular structure turns indeed out to be stable for small values of h. As h was increased the simulation box, initially ($h=0$) of nearly square shape, contracted in the y direction with a slight dilation in the x direction. The ratio of lattice spacings in the y and x directions a_2/a_1, initially equal to $\sqrt{3}$, retained this value up to $h=0.05$, and then progressively decreased ($a_2/a_1=1.70$, 1.60, 1.54, 1.47, and 1.40 at $h=0.1$, 0.2, 0.25, 0.3, and 0.32, respectively) reaching a value of 1 at $h\approx 0.4$. At this value the intralayer first coordination number changed from 2 to 4, typical of a square lattice, while the interlayer first coordination number remained unchanged from its value 4 in the rectangular phase. The transformation from a staggered rectangular to a staggered square lattice is complete at $h=0.5$, and this structure remains stable up to $h\approx 1.05$ (cf. Fig. 1). Confirmation of the staggered square structure is obtained from the order parameter $\Psi_4=0.9$ and peak positions of the nearest-neighbor shells occurring in g_{11} at $r=1.76$ $(=r_1)$, 2.50 $(\sim\sqrt{2}r_1)$, 3.56 $(\sim 2r_1)$, and 3.96 $(\sim\sqrt{5}r_1)$ and in g_{12} at 1.24 $(\sim\sqrt{2}/2r_1)$, 2.80 $(\sim\sqrt{10}/2r_1)$, and 3.76 $(\sim 3\sqrt{2}/2r_1)$.

In the rectangular phase the intralayer energy U_{intra}/NkT decreases from -204.05 at $h=0.05$ to -214.23 at $h=0.5$, and remains nearly constant in the square phase (variation from -214.60 at $h=0.6$ to -214.88 at $h=1.05$ (cf. Fig. 2). The interlayer energy U_{inter}/NkT varies linearly up to $h\approx 0.35$, then increases more slowly in the square phase. Near $h=1.05$ the system starts to transform to a staggered rhombic phase which in turn will evolve, via a first-order transition, into a hexagonal phase at $h\gtrsim 1.24$.

Once the hexagonal ordering is completed the intralayer PDF g_{11} (cf. Fig. 3) and energy ($U_{intra}/NkT=-215.75$ for the 1800 particle system) remain unchanged for all larger separations. Peak positions in g_{11} occur at $r=1.88$ $(=r_1)$, 3.32 $(\sim\sqrt{3}r_1)$, 3.76 $(\sim 2r_1)$, and 4.96 $(\sim\sqrt{7}r_1)$ (cf. Fig. 3); the first coordination number is 6, and the hexatic order parameter is $\Psi_6=0.80$, while $\Psi_4\approx 0$ in accord with a hexagonal crystal structure. Peak positions in the interlayer PDF g_{12} located at $r=1.08$ $(\sim\sqrt{3}/3r_1)$, 2.20 $(\sim 2\sqrt{3}/3r_1)$, and 2.9 $(\sim\sqrt{7/3}r_1)$ (cf. Fig. 3), and a first coordination number of 3,

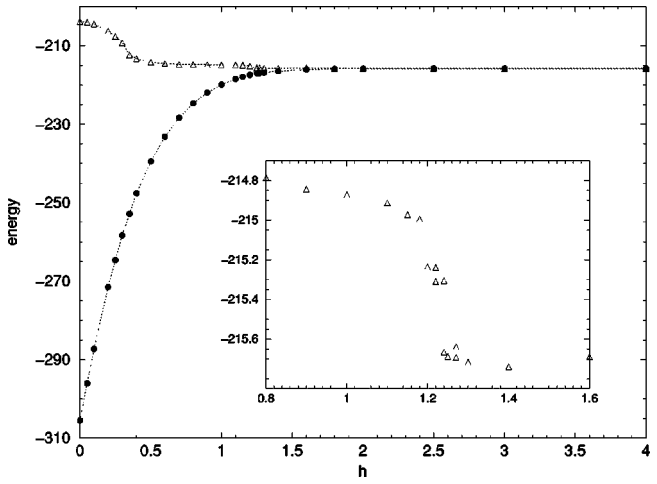

FIG. 2. Energy per particle as a function of layer separation for $\Gamma=196$ and 1800 ions. Filled circles: total energy U/NkT, triangles: intralayer energy U_{intra}/NkT. The inset shows the intralayer energy in the transition region between the square and hexagonal phases. Error bars are of the order of 0.02 except near the phase transition where they can be larger.

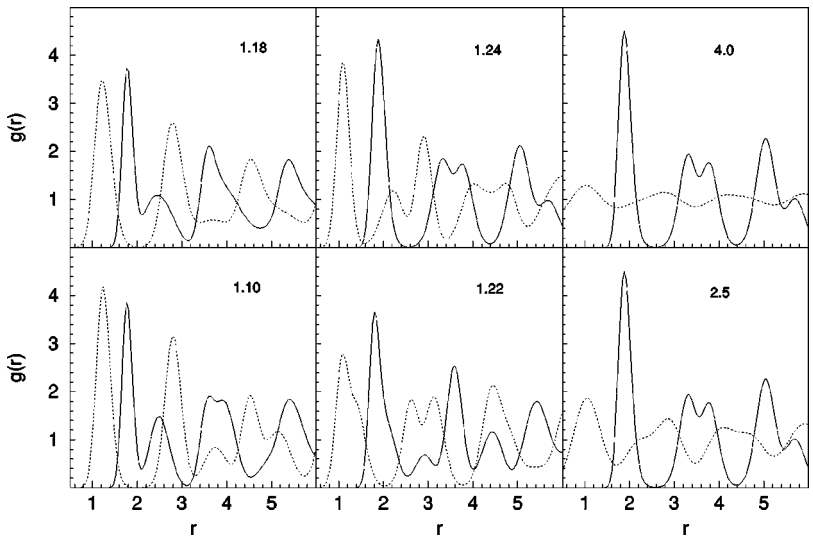

FIG. 3. Intralayer PDF $g_{11}(r)$ (solid line) and interlayer PDF $g_{12}(r)$ (dotted line) at $\Gamma=196$ for $1.1\leqslant h\leqslant 4.0$. Distances are in units of the ion-disk radius a.

further testify to a staggered position of the two layers, i.e., the lattice points of one layer lie directly above the centers of the triangles of the other, thus minimizing the interlayer repulsion. The peaks in g_{12} remain well defined up to $h=2.5$, then slacken, persisting nonetheless up to $h\approx 6$.

Concerning the phase region separating the staggered square and hexagonal phases when, for the 1800 ion system, the layer separation was decreased from $h=1.4$, the system retained its staggered hexagonal structure until, near $h=1.24$, it changed to a linear rhombic structure with lattice vectors of equal lengths 1.8 and angle $\theta\approx 72°$. In accord with such a structure peak positions in g_{11} should therefore occur near $r=1.80$ $(=r_1)$, $(2-2\cos\theta)^{1/2}r_1=2.12$, $(2+2\cos\theta)^{1/2}r_1=2.92$, and $2r_1=3.6$, which can readily be verified from case $h=1.22$ of Fig. 3.

On the other hand, when h was increased from $h=1.05$ in the square phase, we first observed coexistence between regions of both square and rhombic short-range ordering (cf. Fig. 4), as manifested by a broad second peak in g_{11} resulting from the overlap of the preferred second- and third-neighbor positions of the rhombic phase and the second-neighbor position of the square arrangement. Only close to $h=1.22$ did the system achieve a pure rhombic structure, with a lattice angle close to 72°. Upon further increase of the interlayer separation the rhombic structure was found to be mechanically stable beyond the value of $h=1.24$, at which the hexagonal phase became unstable in a reverse sequence of the layer distance variation. Such hysteresis, as well as an abrupt jump of θ from 72° to 60° at the rhombic-hexagonal transition and a discontinuity in the intralayer- and interlayer energies (though to less extent in the total energy) (cf. inset of Fig. 2), plead strongly in favor of a first-order transition in accord with the ground state calculations of Goldoni and Peeters.[2]

Calculations with the smaller number of particles, 512, gave qualitatively similar structures, but shifted the rhombic-hexagonal transition to the somewhat higher value $h\approx 1.27$ and produced lower-energy values, compared to those for the 1800-ion system, for $h>1.1$, with a maximum difference of ≈ 0.4 for $h=3-4$. In fact, for separations $3<h<6$, the sys-

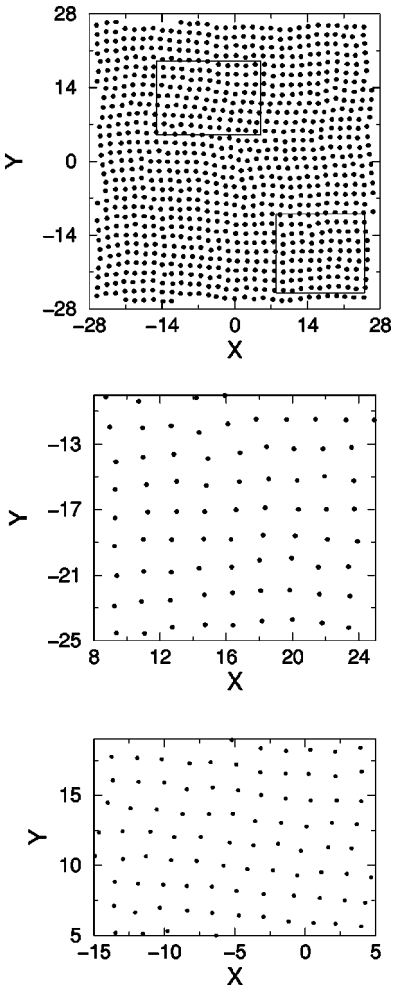

FIG. 4. Snapshot of a layer configuration of 900 ions at $\Gamma=196$ and layer separation $h=1.15$, showing the coexistence of regions with square and rhombic orderings. From top to bottom: full layer, region with square ordering, and region with rhombic ordering. Distances are in units of the ion-disk radius a.

tem showed a preference to adopt a structure in which the two hexagonal layers, though only weakly correlated, were, on average, on top of each other rather than staggered (the nearest neighbor peak in g_{12} was at $r=0$, and subsequent peaks coincided with those in g_{11}). The occurrence of these finite-size effects urged us to resort to a larger system size.

IV. DISCUSSION

We have investigated the solid-solid structural phase transitions arising in a classical bilayer Wigner crystal as a function of layer separation using Monte Carlo simulations in which the box shape can fluctuate, thereby allowing the system to adopt its preferential crystal structure. Between the hexagonal packings of the ions at $h=0$ (single-layer Wigner crystal) and $h \gtrsim 6$ (uncorrelated layers) we identify, for $\Gamma = 196$, four different phases which, in order of increasing h, are the staggered rectangular phase ($0 \lesssim h \lesssim 0.4$), the staggered square phase ($0.5 \lesssim h \lesssim 1.05$), the staggered rhombic phase ($1.05 \lesssim h \lesssim 1.24$), and the staggered hexagonal phase ($1.24 \lesssim h \lesssim 6$).

The use of a simulation cell of variable shape turned out to be particularly efficient for the study of the stable phases for $h \lesssim 1$. The possibility of the aspect ratio L_y/L_x of the simulation box being able to adjust to the ratio of the lattice spacings allowed us to give evidence for the continuous transition from a staggered rectangular phase to a staggered square phase while avoiding the creation of defects. The method is equally efficient for the study of a staggered hexagonal phase to a staggered rhombic phase, where one notes an adjustment of the aspect ratio from $L_y/L_x = 0.86$ (hexagonal) to $L_y/L_x = 0.97-1.01$ (rhombic). In the case of a transition from a square to a rhombic phase, where $L_y/L_x \sim 1.0$ for both phases, the variation of the simulation cell cannot avoid the creation of defects entailing the coexistence of the two phases. However, by allowing one to bypass a free-energy calculation to estimate the stability of the solid phases, the use of a simulation method based on a variable cell shape is equally successful for studying the solid-solid transitions in OCP-like systems as it is those in two- or three-dimensional systems with short-range interactions.[4]

The sequence of phases corresponds to that predicted by Goldoni and Peeters[2] for the ground state ($T=0$ or $\Gamma=\infty$) of the bilayer system. More remarkably, the ranges over which the square and hexagonal phases are stable agree quantitatively with the ground-state calculations ($0.464 < h < 1.102$ for the square phase, and $h > 1.297$ for the staggered hexagonal phase;[2] note that our definition of layer separation differs from that of Refs. 2 and 3 by a factor $\sqrt{\pi}$). Additional MC simulations at $\Gamma = 324$ further indicate a fair degree of insensitivity of the domains of stability of the different phases on Γ (at least away from the melting temperature), in agreement with the finite temperature phase diagram calculated in the harmonic approximation (cf. Fig. 8 of Ref. 2). In contrast, as shown by recent MC simulations by Schweigert *et al.*,[3] the values of Γ at which the different phases melt are not so well estimated in the harmonic approximation. In these more accurate calculations the melting temperature [associated with the temperature at which $U/NT\Gamma$ shows a discontinuity and the translational and orientational order parameters (Ψ_m) vanish] of the square phase at $h=0.5$ is $\approx 35\%$ higher than the melting temperature of the single-layer crystal, while in the hexagonal phase at $h=1.6$ it is $\approx 20\%$ lower. We have obtained rough estimates of the melting temperatures from the values of Γ at which the simulated PDF g_{11} changed from crystal to liquid behavior. Based on this criterion the square phase at $h=0.8$ melts approximately at $\Gamma = 67$, and the staggered hexagonal phase at $h=1.6$ near $\Gamma = 106$. These values for the inverse melting temperature are in excellent agreement with those obtained by Schweigert *et al.*[3] ($\Gamma \sim 66$ and ~ 110, noting that their temperature scale differs from ours by a factor $\sqrt{2}$).

We find good evidence for a first-order rhombic to hexagonal transition with a lattice angle θ jumping discontinuously from $\approx 72°$ to $60°$ near $h=1.24$, in good agreement with the ground-state predictions [a discontinuous drop from $69.48°$ to $60°$ at $h=1.3$ (Ref. 2)], and experimental results of Mitchell *et al.*[10] on laser-cooled trapped $^9Be^+$ ions. It can be noted that a square to hexagonal transition was also observed in bilayer hard-sphere[13] and colloidal[14] systems (particles confined between parallel plates a few particle diameters apart), and that its nature can depend sensitively on the interaction potential. For example, in the case where the particle interaction comprises both a repulsive core-core potential and a narrow attractive part (e.g., colloids) the hexagonal to square lattice transition is found to be first order, and there is no intermediate rhombic phase in contrast with the pure hard-sphere case.[13] Integral equation studies based on the hypernetted-chain equation further show that the various phase behaviors observed in the solid phase as a function of h extend to some degree to the liquid.[11]

The sequence of structural phases observed in the present model system bears close resemblance to the experimental findings by Mitchell *et al.*[10] for a disklike (lenticular) ion plasma of $^9Be^+$ ions in a Penning trap, laser beam cooled to a temperature of a few mK. In this experimental realization of the OCP the confining electric and magnetic fields play the role of the neutralizing background.[12] By using direct imaging techniques, Mitchell *et al.*[10] showed that upon increasing the areal density of the confined ions, the ions in the central part of the ion cloud first crystallize into a one-layer hexagonal structure (the so-called Wigner crystal), then split into a two-layer staggered square before transforming into a two-layer staggered rhombic phase and finally a two-layer staggered hexagonal phase. At some critical density a third layer forms, and the sequence of phase structures repeats.

Comparison between experimental and MC results can be made by identifying, for a given phase, the lattice vector lengths measured experimentally (a_{ex}) and obtained in the MC simulations (a_{MC}). This fixes the length scale (a) used in the simulations. For example, in the experiment the hexagonal phase of the bilayer structure sets in at a density $\sigma_0 a_{WS2D}^2 \approx 0.65$ with a layer separation $h_{ex} \approx 1.35 a_{WS2D}$, where the unit of length is taken to be $a_{WS2D} = 10.7$ μm. At this density the lattice vector length a_{ex} related to the central area density σ_0, lattice angle θ, and number of lattice planes n by $a_{ex} = \sqrt{\sin\theta \sigma_0 / n}$ is $\approx 1.885 a_{WS2D}$ which, when identi-

fied with the MC value $a_{MC}=1.88a$, as given from the nearest-neighbor distance in the hexagonal phase, leads to $a=1.0027a_{WS2D}$ and consequently $h_{ex}/a=1.346$, in good agreement with the Monte Carlo result $h_{MC}/a\approx 1.3$. Similar agreement is found in the square phase. In addition the scale for a allows one to determine an absolute temperature which for $\Gamma=196$ is $T=e^2/\Gamma ka=7.95$ mK (k is the Boltzmann constant), compatible with experiment (<10 mK).

ACKNOWLEDGMENTS

Computing time on the CRAY C-98 was granted by the Institut de Développement et de Ressources en Informatique (IDRIS). S.J. acknowledges financial support from the Universidad Complutense de Madrid, and the Spanish Dirección General de Enseñanza Superior e Investigación Científica under Grant No. PB97-0258. She also wants to thank the Laboratoire de Physique Théorique for its kind hospitality.

[1] See, e.g., G. J. Kalman, K. B. Blagoev, Z. Donko, K. I. Golden, G. McMullan, V. Valtchinov, and H. Zhao, J. Phys. IV **10**, 85 (2000).
[2] G. Goldoni and F. M. Peeters, Phys. Rev. B **53**, 4591 (1996).
[3] I. V. Schweigert, V. A. Schweigert, and F. M. Peeters, Phys. Rev. Lett. **82**, 5293 (1999).
[4] M. Parrinello and A. Rahman, Phys. Rev. Lett. **45**, 1196 (1980).
[5] S. Yashonath and C. N. R. Rao, Mol. Phys. **54**, 245 (1985).
[6] E. L. Lieb and H. Narnhofer, J. Stat. Phys. **12**, 291 (1975).
[7] See, e.g., B. Cichocki and B. U. Felderhof, Mol. Phys. **67**, 1373 (1973).
[8] C. G. Grimes and G. Adams, Phys. Rev. B **42**, 795 (1979).
[9] R. C. Gann, S. Chakravarti, and G. V. Chester, Phys. Rev. B **20**, 326 (1979); R. H. Morf, Phys. Rev. Lett. **43**, 931 (1979); R. K. Kalia, P. Vashishta, and S. W. de Leeuw, Phys. Rev. B **23**, 4794 (1981); S. Muto and H. Aoki, *ibid.* **59**, 14 911 (1999).
[10] T. B. Mitchell, J. J. Bollinger, D. H. E. Dubin, X.-P. Huang, W. M. Itano, and R. H. Baughman, Science **282**, 1290 (1998).
[11] V. I. Valtchinov, G. Kalman, and K. B. Blagoev, Phys. Rev. E **56**, 4351 (1997).
[12] J. H. Malmberg and T. M. O'Neil, Phys. Rev. Lett. **39**, 1333 (1977).
[13] M. Schmidt and H. Löwen, Phys. Rev. Lett. **76**, 4552 (1996).
[14] R. Zangi and S. A. Rice, Phys. Rev. E **61**, 671 (2000).